J. Fluid Mech. (1990), *vol.* 216, *pp.* 613–628
Printed in Great Britain

New phenomena in the Eckhaus instability of thermal Rossby waves

By A. C. OR†
Division of Applied Sciences, Harvard University, Cambridge, MA 02138, USA

(Received 21 October 1988 and in revised form 15 December 1989)

An analytical study on the Eckhaus instability of moderately nonlinear thermal Rossby waves is developed. A solvability condition of the lowest order is derived. The condition not only produces results that agree reasonably well with the earlier Galerkin formulation, but also leads to some new findings that are otherwise difficult to discover by the previous method. Over a wide range of parameters, this paper reports the existence of a branch of the stability limit that corresponds to a pair of disturbances with a finite, rather than an infinitesimal wavenumber modulation. As the Prandtl number tends to a small value, the asymmetry between the two branches of the stability limit becomes very pronounced, which is manifested as a severely distorted stability region.

1. Introduction

Convection rolls in a rapidly rotating system with slanted end boundaries can be realized in the form of thermal Rossby waves. The existence of these wave modes has been demonstrated through both analytical and experimental studies. The waves are of significance in the context of geophysical and astrophysical applications since the latter are typically characterized by the release of buoyancy energy under the influence of rapid rotation. Since the waves can also give rise to orderly mean flows through their fluctuating motion, they offer a widely acceptable mechanism for explaining the large-scale mean flows in the Earth's core and in the major planets' atmospheres. For an extensive review on the subject, readers are referred to Busse (1982). Under laboratory conditions, the waves can be realized in a rapidly rotating cylindrical annulus with slanted end boundaries, where the centrifugal force replaces the role of the gravity force (see Busse & Carrigan 1975; Azouni, Bolton & Busse 1986). The laboratory realization of the waves further stimulates the desire to understand the hydrodynamic stability properties, which might eventually enhance our knowledge on the problem of transition to turbulence. In two of the previous surveying papers, Busse & Or (1986) and Or & Busse (1987), many bifurcation and instability properties of the waves have been identified. In particular, an unusual Eckhaus instability was briefly reported. Since such a phenomenon appears new, and it does not seem to be found in any other better-known pattern-forming systems, it is of interest that this instability be studied in further detail.

Eckhaus instability is of general interest to fluid dynamicists on account of its common occurrence in continuous periodic systems, and its close relationship with the wavelength changing process. Studies of the instability has appeared in

† Present address: Hughes Aircraft Company, S&CG, Bldg. S41, M/S B320, P.O. Box 92919, CA 90009, USA.

numerous papers. In several better-known fluid systems, some of the references available are: Eckhaus (1965), Kogelman & DiPrima (1970), Nakaya (1974), Riecke & Paap (1985)) on Taylor vortex flows; Newell & Whitehead (1969), Busse (1971), Busse & Bolton (1984) on Rayleigh–Bénard convection; and Benjamin & Feir (1967) on Stokes waves. Eckhaus was the first author who studied the instability. Several others had also identified the fundamental role played by the instability in pattern forming, notably Kogelman & DiPrima (1970), Stuart & DiPrima (1978) and Kramer & Zimmerman (1985). In particular, in the work of Stuart & DiPrima, a unifying treatment of the instability was applied to both Taylor vortex flows and Stokes waves. Their work shows that the physical mechanism that gives rise to Benjamin–Feir resonance, or the so-called sideband instability, is identical to that which gives rise to the Eckhaus instability in Taylor vortex flow. Among all the previous studies, perhaps the most celebrated result is implied by the following stability criterion:

$$|\alpha-\alpha_c| < \frac{1}{\sqrt{3}}|\alpha_0-\alpha_c|, \tag{1.1}$$

The above condition asserts that the bandwidth of the wavenumber of the stable nonlinear solutions is $1/\sqrt{3}$ of the bandwidth of existence of the solutions. From (1.1), the two branches of the stability limit are symmetrical about the critical condition. Even more remarkable is that while the derivation of the analytical limit is based on the lowest-order theory, such a limit continues to be valid, at least qualitatively, even when the control parameter becomes far away from the critical condition.

In the paper by Or & Busse (1987) the fully nonlinear numerical results are based on a Galerkin formulation, which solves a full truncated eigenvalue problem. The results show that the right-hand branch ($\alpha > a_c$) of the stability limit is associated with a finite, rather than an infinitesimal value d^*. Here d^* denotes the limiting value of the wavenumber modulation, or the Floquet parameter.

In this paper, this unusual phenomenon will be further explored by means of an analytical theory. In §2, the mathematical formulation for the instability problem is developed. Instead of solving the full eigenvalue problem, the lowest-order solvability condition based on an amplitude expansion is derived. Such a condition not only permits room for more physical insight, but also is more efficient in terms of computation for obtaining stability curves. In §3, the growth-rate properties are studied. In particular, the analytical results are compared with the Galerkin results so as to validate the former. In the analytical treatment, we also reproduce the stability limit for the ordinary convection rolls in the limit $\eta^* = 0$. Such a limit which includes the first-order asymmetry was first derived by Busse & Bolton (1984). For the thermal Rossby regime, the solvability condition is further simplified to permit derivations of the growth rate coefficients based on the perturbation expansion in some asymptotic limits. In §4, we conclude the paper with a few remarks and discussions.

2. The solvability condition

A fluid-filled cylindrical annulus as shown in figure 1 is considered. The annulus rotates about its axis of symmetry with angular velocity $\boldsymbol{\Omega}$. The inner and outer walls are kept at constant temperatures of T_1 and T_2 respectively. The gap width D is used

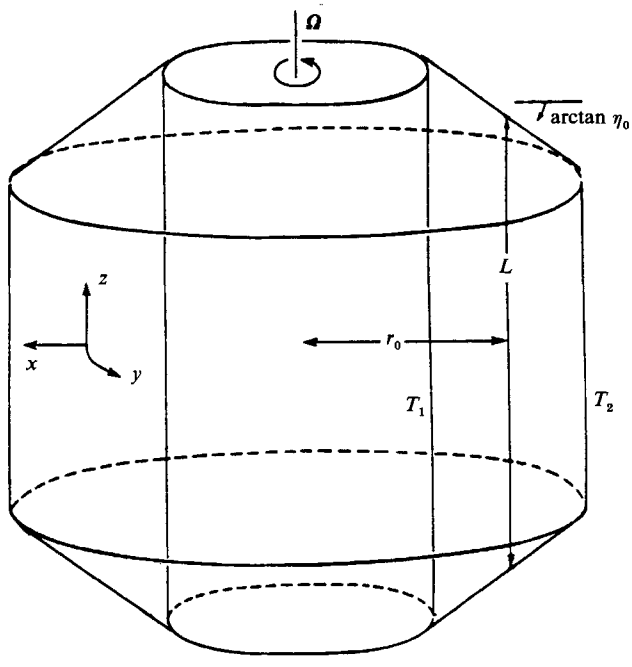

FIGURE 1. The cylindrical annulus apparatus with conical end boundary.

as the scale for length; D^2/ν as the scale for time, where ν is the kinematic viscosity; and $P(T_1-T_2)$ as the scale for temperature. The full derivation of the basic equations from the Navier–Stokes and the heat equation was given in Busse & Or (1986). These basic equations are

$$\left.\begin{aligned}(\partial_t-\nabla^2)\nabla^2\psi-\eta^*\partial_y\psi+R\partial_y\theta &= J(\psi,\nabla^2\psi),\\ (P\partial_t-\nabla^2)\theta+\partial_y\psi &= PJ(\psi,\theta),\end{aligned}\right\} \tag{2.1}$$

subject to the free-slip boundary conditions

$$\psi=\partial_{xx}^2\psi=\theta=0, \quad x=-\tfrac{1}{2},\tfrac{1}{2}.$$

In (2.1), $\nabla^2\equiv\partial_{xx}^2+\partial_{yy}^2$, and J denotes the Jacobian. The non-dimensional parameters are defined as follows:

Prandtl number $$P\equiv\frac{\nu}{\kappa},$$

Rayleigh number $$R\equiv\frac{\gamma D^3\Omega^2 r_0(T_2-T_1)}{\nu\kappa},$$

Coriolis number $$\eta^*\equiv\frac{4\eta_0}{lE},$$

Ekman number $$E\equiv\frac{\nu}{\Omega D^2},$$

where κ, γ, r_0, l and η_0 are respectively the thermal diffusivity, the coefficient of thermal expansion, the mean radius and the mean length of the annulus, and the

tangent of the angle between the conical end surface and the equatorial plane. The finite-amplitude solutions, at their lowest order of amplitude, have the form

$$\left.\begin{aligned}
\psi &= A\sin\pi(x+\tfrac{1}{2})\sin(\alpha y+\omega t)+O(A^3),\\
\theta &= -\alpha A\sin\pi(x+\tfrac{1}{2})\frac{P\omega\sin(\alpha y+\omega t)+\Delta\cos(\alpha y+\omega t)}{\Delta^2+P^2\omega^2}\\
&\quad+\frac{A^2P\alpha^2\Delta\sin 2\pi(x+\tfrac{1}{2})}{8\pi(\Delta^2+P^2\omega^2)}+O(A^3),\\
R &= R_0\left(1+\frac{A^2P^2\alpha^2\Delta}{8(\Delta^2+P^2\omega^2)}+O(A^4)\right),\quad \omega=\omega_0+O(A^4),
\end{aligned}\right\} \tag{2.2}$$

where $$R_0=\frac{\Delta(\Delta^2+P^2\omega_0^2)}{\alpha^2},\quad \omega_0=-\frac{\eta^*\alpha}{(1+P)\Delta},\quad \Delta\equiv(\pi^2+\alpha^2).$$

In the above expressions, A is the amplitude of motion, α is the wavenumber of the waves, and ω is the frequency. The finite-amplitude solutions thus have an existence region where $R\geqslant R_0(\alpha)$ for a given α. To investigate the Eckhaus instability of (2.2), we superimpose infinitesimal disturbances of the form

$$\left.\begin{aligned}
\tilde{\psi} &= (\tilde{\psi}_0+A\tilde{\psi}_1+A^2\tilde{\psi}_2+\ldots)\exp(\sigma t),\\
\tilde{\theta} &= (\tilde{\theta}_0+A\tilde{\theta}_1+A^2\tilde{\theta}_2+\ldots)\exp(\sigma t)
\end{aligned}\right\} \tag{2.3}$$

to the basic solution; where $\tilde{\psi},\tilde{\theta}$ satisfy

$$(\partial_t-\nabla^2)\nabla^2\tilde{\psi}-\eta^*\partial_y\tilde{\psi}+R\,\partial_y\tilde{\theta}=J(\tilde{\psi},\nabla^2\psi)+J(\psi,\nabla^2\tilde{\psi}), \tag{2.4a}$$

$$(P\,\partial_t-\nabla^2)\tilde{\theta}+\partial_y\tilde{\psi}=PJ(\tilde{\psi},\theta)+PJ(\psi,\tilde{\theta}) \tag{2.4b}$$

in the linear approximations. Here we are only interested in a pair of disturbances that correspond approximately to the translational neutral mode of the basic wave solutions, but have slightly modulated wavenumbers. Anticipating that the growing disturbance has a growth rate σ of the order A or smaller, we obtain the zeroth-order solutions $\tilde{\psi}_0$ and $\tilde{\theta}_0$ as

$$\left.\begin{aligned}
\tilde{\psi}_0 &= \sin\pi(x+\tfrac{1}{2})\sum_{n=1}^{2}C^{(n)}\exp[\mathrm{i}(-1)^n(\alpha_n y+\omega_n t)],\\
\tilde{\theta}_0 &= -\sin\pi(x+\tfrac{1}{2})\sum_{n=1}^{2}C^{(n)}\frac{\mathrm{i}(-1)^n\alpha_n}{\Delta_n+\mathrm{i}(-1)^nP\omega_n}\exp[\mathrm{i}(-1)^n(\alpha_n y+\omega_n t)],
\end{aligned}\right\} \tag{2.5}$$

where $\alpha_n\equiv\alpha+(-1)^n d$, $\omega_n=\omega+(-1)^n\omega' d$. The prime here denotes the derivative taken with respect to α. Expression (2.5) satisfies (2.4) at the zeroth order. The higher-order deviations are assumed of the order of A^3, which will be accounted for

as soon as the solvability condition becomes available. In the next order balance, $\tilde{\psi}_1$ and $\tilde{\theta}_1$ can be determined, given by

$$\left.\begin{aligned}
\tilde{\psi}_1 &= d\sin 2\pi(x+\tfrac{1}{2})\sum_{n=1}^{2}(-1)^n f_n C^{(n)}\exp[\mathrm{i}(dy+\omega' dt)],\\
\tilde{\theta}_1 &= -\mathrm{i}\sin 2\pi(x+\tfrac{1}{2})\sum_{n=1}^{2}(-1)^n g_n C^{(n)}\exp[\mathrm{i}(dy+\omega' dt)],\\
f_n &= \pi(\alpha+\alpha_n)[(\alpha+\alpha_n)(\mathrm{i}P\omega' d^2+4\pi^2+d^2)+PR_0H_n]/4D,\\
g_n &= \pi(\alpha+\alpha_n)[d^2(\alpha+\alpha_n)+P((4\pi^2+d^2)^2+\mathrm{i}\omega' d(4\pi^2+d^2)+\mathrm{i}\eta^* d)H_n]/4D,\\
H_n &= \frac{\alpha_n}{\Delta_n+\mathrm{i}P(-1)^n\omega_n}+\frac{\alpha}{\Delta-\mathrm{i}P(-1)^n\omega},\\
D &= d^2R_0-(4\pi^2+d^2+\mathrm{i}P\omega' d)[(4\pi^2+d^2)^2+\mathrm{i}\eta^* d+\mathrm{i}(4\pi^2+d^2)\omega' d].
\end{aligned}\right\} \quad (2.6)$$

These expressions have been derived in full without having to assume that d is small. In (2.6) the second harmonic modes of α have not been included. These modes can be shown to be much weaker and are therefore ignored.

To obtain solvability condition from the next order balance, we must introduce the adjoint homogeneous problem of (2.4). We obtain

$$\psi^* = \sin\pi(x+\tfrac{1}{2})\exp[-\mathrm{i}(-1)^m(\alpha_m y+\omega_m t)], \quad \theta^* = -\frac{\mathrm{i}\alpha_m(-1)^m\psi^*}{\Delta_m+\mathrm{i}(-1)^m P\omega_m}, \quad (2.7)$$

where $m = 1, 2$ and the asterisk denotes the adjoint solutions. We multiply (2.4a) by $\Delta_m^{-1}\psi^*$ and (2.4b) by $\Delta_m^{-1}R_m\theta^*$, where $R_m = \Delta_m(\Delta_m^2+P^2\omega_m^2)/\alpha_m^2$; add and average the result over the fluid annulus; and obtain the secular terms in the form of a 2×2 system with unknowns $C^{(n)}, n = 1, 2$:

$$\begin{aligned}
\sum_{n=1}^{2} C^{(n)}\Bigg\{&\left[\sigma\left(1+\frac{P(\Delta_m^2+P^2\omega_m^2)}{(\Delta_m+\mathrm{i}(-1)^m P\omega_m)^2}\right)-r_m+s_m\right]\delta_{nm}+\tfrac{1}{4}\pi A^2\left(\frac{\alpha+\alpha_m}{\Delta_m}\right)\\
&\times\left[\frac{(\Delta-4\pi^2-d^2)}{(\Delta_m-\mathrm{i}(-1)^m P\omega_m)}+\frac{P\alpha_m R_m\Delta}{\alpha R_0(\Delta_m+\mathrm{i}(-1)^m P\omega_m)}\right](\Delta_m-\mathrm{i}(-1)^m P\omega_m)f_n(-1)^n d\\
&-\tfrac{1}{4}\pi A^2\left(\frac{\alpha+\alpha_m}{\alpha_m}\right)P(\Delta_m-\mathrm{i}P(-1)^m P\omega_m)(-1)^{m+n}g_n\Bigg\} = 0, \quad (2.8)
\end{aligned}$$

where

$$r_m = \left(\frac{R_0}{R_m}-1\right)(\Delta_m-\mathrm{i}P(-1)^m\omega_m), \quad s_m = \frac{P^2\Delta^2\alpha_m^2A^2}{8\Delta_m(\Delta_m+\mathrm{i}P(-1)^m\omega_m)}\left(\frac{R_m}{R_0}-1\right).$$

The term r_m represents the real part of the remainder from the zeroth-order balance; the term s_m comes from the difference between linear terms $-P\,\partial_y\tilde{\psi}_0\,\partial_x\bar{\theta}$ and $(R-R_0)\,\partial_y\tilde{\theta}_0$. Since s_m is roughtly a factor of $R-R_0/R_0$ smaller than r_m, the former can be safely ignored even in the moderately nonlinear region. The solvability condition (2.8) then consists of a balance between r_m and the secular terms generated by nonlinearity. It is noted that the imaginary part of the remainder from the zeroth order, $\mathrm{i}(-1)^m(1+P)(\omega(\alpha_m)-\omega_m)$ (where $\omega(\alpha_m)$ is the wave frequency at α_m), varies on the order A^4 and is excluded from the present solvability condition. The subsequent analysis and the comparisons with the fully nonlinear results suggest that for all purposes, the lowest-order solvability condition appears sufficient to account for the instability.

3. Growth-rate analysis

It is desirable to simplify condition (2.8) so that it reveals the dominant effects of the instability. We proceed in the following order: first, a simpler equation is sought without removing any of the essential effects; secondly, a stability criterion in the limit of ordinary convection rolls is reproduced; thirdly, a perturbation expansion on the growth rate is developed, such that the growth-rate coefficients are derivable from some asymptotic limits; lastly, a comparison between the analytical and the fully nonlinear result is provided.

Assuming $d \ll \alpha$, it is convenient to express condition (2.8) by a Taylor expansion in d/α. All the terms in (2.8) are Taylor-expanded in d/α, except the term D in which higher-order contributions can be large. After manipulating through algebra and by retaining only the first-order terms, condition (2.8) is simplified to

$$\sum_1^2 \left\{ [q_m \sigma - r_m]\,\delta_{nm} + (-1)^{m+n} A^2 G_m \times \left[1 + \frac{d}{\alpha}(\mathrm{i}\eta^{(0)} + (\eta_m^{(1)} + \eta_m^{(3)})(-1)^m + \eta_n^{(2)}(-1)^n)\right]\right\} C^{(n)} = 0, \quad (3.1)$$

where
$$q_m = 1 + \frac{P(\Delta^2 + P^2\omega^2)}{(\Delta + \mathrm{i}(-1)^m P\omega)^2}; \quad G_m = -\frac{8P^2\pi^6\Delta^2}{DR_0}(\Delta - \mathrm{i}(-1)^m)\,P\omega,$$

$$\eta_m^{(1)} = -\frac{\alpha^2 R_0}{16\pi^2\Delta^3}\left[\left(\frac{\Delta - 4\pi^2}{\Delta - \mathrm{i}(-1)^m P\omega}\right)P^{-1} + \frac{\Delta}{\Delta + \mathrm{i}(-1)^m P\omega}\right]\left(4\alpha^2 P^{-1} + \frac{\Delta^2}{\pi^2}\right),$$

$$\eta_n^{(2)} = \frac{1}{2} + \frac{(\Delta - \mathrm{i}(-1)^n P\omega)}{2\Delta}\left(1 - \frac{\alpha(2\alpha + \mathrm{i}P\omega')}{\Delta + \mathrm{i}(-1)^n P\omega}\right),$$

$$\eta_m^{(3)} = \left(-\frac{1}{2} + \frac{\alpha(2\alpha - \mathrm{i}P\omega')}{\Delta - \mathrm{i}(-1)^m P\omega}\right); \quad \eta^{(0)} = \frac{\alpha}{16\pi^4}(4\pi^2\omega' + \eta^*).$$

Equation (3.1) appears simpler. It has the property that the quantities with subscripts 1 and 2 are conjugate with each other. The term $\eta^{(0)}$ comes from a phase-shifted term in g_n that is proportional to d. The term $\eta_m^{(1)}$ comes from $f_n d$. For large η^*, the terms $\eta_n^{(2)}$ and $\eta_m^{(3)}$ are much smaller than $\eta^{(0)}$ and $\eta_m^{(1)}$. They are of the order of $(\alpha_n - \alpha)$ and $(\alpha_m - \alpha)$ and come from the expansion of g_n. Below we shall first consider the case of ordinary convective rolls.

3.1. *Ordinary convective rolls*

For $\eta^* = 0$, (2.6) and (3.1) evaluated at $\alpha = \alpha_c = \pi/\sqrt{2}$ become

$$\left.\begin{aligned} f_n &= -\frac{P}{32\pi}(P^{-1} + \tfrac{9}{8}); \quad g_n = -\frac{P}{12\pi}\left(1 + \tfrac{2}{3}(-1)^n \frac{d}{\alpha}\right), \\ G_m &= G = \frac{P^2\pi^2}{16}; \quad \eta_m^{(1)} = \eta^{(1)} = -\frac{1}{8}\left(1 - \frac{5}{3P}\right)(P^{-1} + \tfrac{9}{8}), \\ \eta_m^{(2)} &= \eta^{(2)} = \tfrac{2}{3}, \quad \eta_m^{(3)} = \eta^{(3)} = \tfrac{1}{6}, \quad r_m = \frac{\alpha_m^2}{\Delta_m^2}(R_0 - R_m). \end{aligned}\right\} \quad (3.2)$$

Further simplification of r_m by expanding in d gives

$$r_m = -4\left[(-1)^m(\alpha-\alpha_c)\,d\left(2-\left(\frac{\alpha-\alpha_c}{\alpha}\right)\right)+d^2\left(1-\left(\frac{\alpha-\alpha_c}{\alpha}\right)\right)\right] \tag{3.3}$$

Thus the solvability condition (3.1) becomes

$$(1+P)^2\sigma^2-(1+P)\,\sigma(r_1+r_2-2A^2G)+r_1r_2-A^2G$$
$$\times\left[r_1+r_2+(\eta^{(1)}+\eta^{(2)}+\eta^{(3)})\,(r_1-r_2)\frac{d}{\alpha}\right]-4A^4G^2(\eta^{(1)}+\eta^{(3)})\,\eta^{(2)}\left(\frac{d}{\alpha}\right)^2=0. \tag{3.4}$$

Equation (3.4) is identical to (2.11) of Busse & Bolton (1984). To facilitate a comparison between our results and theirs, we note that their notation $(x, z, -d, \partial_x\phi, \theta, \nabla^2, A_2)$ corresponds to our $(y, x, d, \psi, R\theta, A_2, \partial_{yy}^2)$. From (2.2), we also have $9\pi^2A^2G = (R-R_0)$. Anticipating σ in (3.4) to be of the order of d^2, we conclude that the leading-order balance comes from $(1+P)A^2G\sigma$ and the constant term. Hence the leading-order expression for σ is

$$\sigma=\left(\frac{4d^2}{1+P}\right)\left[18\pi^2(\alpha-\alpha_c)^2\left(3-\frac{(\alpha-\alpha_c)}{\alpha}\left(\frac{97}{144}-\frac{7}{16P}-\frac{5}{6P^2}\right)\right)-(R-R_c)\right]$$
$$\times[(R-R_c-18\pi^2(\alpha-\alpha_c)^2)]^{-1}. \tag{3.5}$$

Condition (3.5) reproduces the same stability region as Busse & Bolton's, up to the first order of asymmetry effects in $\alpha-\alpha_c$. Since both the present and previous studies indicate that the higher-order effects contribute negatively to σ, the instability is indeed sufficiently determined by the leading-order expression (3.5). Next, let us consider the regime of thermal Rossby waves.

3.2. *Thermal Rossby waves*

3.2.1. *The perturbation scheme*

Equation (3.1) can be re-expressed in the form of a quadratic equation in σ, which is

$$q_1q_2\sigma^2+[-q_1r_2-q_2r_1+A^2(q_1G_2+q_2G_1)]\,\sigma+r_1r_2$$
$$-r_1A^2G_2\left[1+\frac{d}{\alpha}(i\eta^{(0)}+\eta_2^{(1)})\right]-r_2A^2G_1\left[1+\frac{d}{\alpha}(i\eta^{(0)}-\eta_1^{(1)})\right]=0. \tag{3.6}$$

The $O(A^4)$ contribution to the equation can be shown to be small and therefore is neglected. For the regime of interest, especially one that is relevant for geophysical applications, η^* is of the order of 10^3 or higher. Independent of the Prandtl number, the terms $\eta_n^{(2)}$ and $\eta_m^{(3)}$ can also be neglected since they are at least an order of magnitude smaller than $\eta^{(0)}$ and $\eta_m^{(1)}$. with some algebraic manipulation, (3.6) can be rewritten in the form

$$a\sigma^2+b\sigma+c=0, \tag{3.7}$$

where its coefficients are expanded in d,

$$a=a_0+ia_1d+a_2d^2,$$
$$b=b_0+ib_1d+b_2d^2+ib_3d^3+b_4d^4,$$
$$c=c_2d^2+ic_3d^3+c_4d^4+ic_5d^5+c_6d^6,$$
$$\sigma=\sigma_2d^2+i\sigma_3d^3+\sigma_4d^4+i\sigma_5d^5+\sigma_6d^6+\ldots.$$

Before showing the expressions for the expansion coefficients, we note that all of the coefficients are real. Furthermore, the even and odd powers are consistent with the

property that $\sigma(d) = \sigma^*(-d)$ (here the asterisk denotes complex-conjugate). The expressions for the coefficients are

$$
\left.\begin{aligned}
&a_0 = 1-\tfrac{2}{3}P+P^2, \quad a_1 = \mu_1(1-\tfrac{2}{3}P+P^2), \quad a_2 = \mu_2(1-\tfrac{2}{3}P+P^2),\\
&b_0 = \frac{2\Delta_c}{R_c}(1+P)\hat{A}^2, b_1 = -\frac{2\beta}{R_c}P(1-P)\,\omega_c(\alpha-\alpha_c)\\
&\quad+\frac{2\Delta_c}{R_c}(1+P)\left(\frac{4\pi^2\omega'+\eta^*}{16\pi^4}\right)\hat{A}^2+\frac{\alpha_c}{\Delta_c^3}\left(\frac{4\alpha_c^2}{P}+\frac{\Delta_c^2}{\pi^2}\right)\left(\frac{\Delta_c P\omega_c}{\Delta_c^2+P^2\omega_c^2}\right)\hat{A}^2,\\
&b_2 = \frac{\beta}{R_c}(2P(1-P)\,\omega_c\mu_1(\alpha-\alpha_c)+(1+P)\,\Delta_c),\\
&b_3 = \frac{\beta}{R_c}(-2P(1-P)\,\omega_c\mu_2(\alpha-\alpha_c)+\mu_1(1+P)\,\Delta_c),\\
&b_4 = \frac{\beta}{R_c}(\mu_2(1+P)\,\Delta_c), \quad c_2 = \frac{\beta(\Delta_c^2+P^2\omega_c^2)}{R_c^2}\Big[-\beta(\alpha-\alpha_c)^2+\hat{A}^2\\
&\quad\times\left(1+\frac{R_c\alpha_c}{8\pi^2\Delta_c^2(\Delta_c^2+P^2\omega_c^2)}\left(\frac{4\alpha_c^2}{P}+\frac{\Delta_c^2}{\pi^2}\right)\left(\frac{\Delta_c-4\pi^2}{P}+\Delta_c\right)(\alpha-\alpha_c)\right)\Big],\\
&c_3 = -\mu_1\frac{\beta^2}{R_c^2}(\Delta_c^2+P^2\omega_c^2)\,(\alpha-\alpha_c)^2+\frac{\beta}{R_c^2}\hat{A}^2\Big[(\Delta_c^2+P^2\omega_c^2)\left(\frac{4\pi^2\omega'+\eta^*}{16\pi^4}\right)\\
&\quad-\frac{\alpha_c R_c P\omega_c}{16\pi^2\Delta^3}\left(\frac{4\alpha_c^2}{P}+\frac{\Delta_c^2}{\pi^2}\right)\left(\frac{\Delta_c-4\pi^2}{P}-\Delta_c\right)\Big],\\
&c_4 = \frac{\beta^2(\Delta_c^2+P^2\omega_c^2)}{R_c^2}(\tfrac{1}{4}-\mu_2(\alpha-\alpha_c)^2),\\
&c_5 = \mu_1\frac{\beta^2(\Delta_c^2+P^2\omega_c^2)}{4R_c^2}, \quad c_6 = \mu_2\frac{\beta^2(\Delta_c^2+P^2\omega_c^2)}{4R_c^2},
\end{aligned}\right\} \tag{3.8}
$$

where

$$
\hat{A}^2 = \tfrac{1}{8}P^2\Delta_c^2A^2, \quad r_n = \frac{\beta}{R_c}(\Delta_c+\mathrm{i}P\omega_c)\,[-(-1)^n\,(\alpha-\alpha_c)\,d-\tfrac{1}{2}d^2], \quad \beta = R_c''.
$$

The μ_n terms come from expanding D, where $D = -64\pi^6(1+\mathrm{i}\mu_1 d+\mu_2 d^2)$; their expressions are

$$
\mu_1 = \frac{1}{16\pi^4}(4\pi^2(1+P)\,\omega'+\eta^*), \quad \mu_2 = \frac{-1}{64\pi^6}(R_c+P\omega'(\eta^*+4\pi^2\omega')).
$$

Expressions (3.8) come from the leading-order terms of the Taylor expansion in d about the critical condition. Since (3.7) is complex, its solutions in closed-form do not produce any simple expressions for the instability criterion. The quadratic equation, however, can be efficiently solved on a computer. Alternatively, if we assume that $d \ll \alpha-\alpha_c$ and A is finite, then proceeding on the expansion scheme as outlined in (3.7) the equation yields the following sequence of equations:

$$
\left.\begin{aligned}
&b_0\sigma_2+c_2 = 0,\\
&b_0\sigma_3+c_3+b_1\sigma_2 = 0,\\
&b_0\sigma_4+a_0\sigma_2^2-b_1\sigma_3+b_2\sigma_2+c_4 = 0,\\
&b_0\sigma_5+a_0\sigma_2\sigma_3+a_1\sigma_2^2+b_1\sigma_4+b_2\sigma_3+b_3\sigma_2+c_5 = 0,\\
&b_0\sigma_6-a_0\sigma_3^2-a_1\sigma_2\sigma_3+a_2\sigma_2^2-b_1\sigma_5+b_2\sigma_4-b_3\sigma_3+b_4\sigma_2+c_6 = 0.
\end{aligned}\right\} \tag{3.9}
$$

While the expansion scheme is advantageous in providing useful results, it is cautioned that such a scheme may only be valid for a sufficiently small value of d, that is within the radius of convergence of the series. An estimate of the radius of convergence can be obtained by comparing successive terms in the series.

3.2.2. *Analytical result*

From (3.9) and the expression of c_2 in (3.8), we obtain

$$\sigma_2 = \frac{\beta\alpha_c^2}{2\Delta_c^2(1+P)}\hat{A}^{-2}\left[\beta(\alpha-\alpha_c)^2+\hat{A}^2\left(1+\kappa\left(\frac{\alpha-\alpha_c}{\alpha_c}\right)\right)\right], \tag{3.10a}$$

where $\kappa = \frac{\alpha_c^2}{8\pi^2}\left(\frac{4}{P}+\frac{\Delta_c^2}{\pi^2\alpha_c^2}\right)\left[1+P^{-1}\left(1-\frac{4\pi^2}{\Delta_c}\right)\right]$, $\hat{A}^2 = (R-R_c)-\frac{1}{2}\beta(\alpha-\alpha_c)^2$.

The corresponding stability region is given by

$$R-R_c \geqslant \frac{\beta(\alpha-\alpha_c)^2}{2\left[1+\kappa\left(\frac{\alpha-\alpha_c}{\alpha_c}\right)\right]}\left[3+\kappa\left(\frac{\alpha-\alpha_c}{\alpha_c}\right)\right]. \tag{3.10b}$$

For $\eta^* = 0, \beta = 36\pi^2$, (3.10$b$) reproduces the same stability region of ordinary convection to the leading order as that determined by (3.5). The small difference between the two expressions is due to the ignoring of $\eta_n^{(2)}$ and $\eta_m^{(3)}$ for the present case. For η^* of the order of 10^3 or larger, the asymmetry term $(\alpha-\alpha_c)/\alpha_c$ in (3.10b) exerts a strong influence. Such an effect is evident from figure 3 below where $\kappa > 0$ (see the left-hand branch dashed curve and the right-hand branch dotted curve).

A close examination of the expression for κ in (3.10a) reveals an even more interesting property, namely, κ becomes negative when

$$\left(\frac{\alpha_c}{\pi}\right)^2 \leqslant \frac{3-P}{1+P} \tag{3.11}$$

independent of the value of η^*. Since the existence of solutions requires $\alpha_c > \pi/\sqrt{2}$, condition (3.11) only can be satisfied for α_c if $P \leqslant \frac{5}{9}$. In particular, as $P \to 0$, condition (3.11) requires $\alpha_c \leqslant \sqrt{3}\pi$. Typically, for P of order unity, α_c is of the order of $\eta^{*\frac{1}{5}}$ as $\eta^* \to \infty$. But even for large η^*, if P is small enough, α_c can remain of order unity such that κ is negative. In this case (3.11) can still be satisfied. As $P \to 0$, κ becomes very large since it varies as P^{-2}. Thus for small P, the two branches of the stability limit can be severely distorted. This is typically what figure 5 shows. Indeed close to the critical condition, the branches are shifted to the left. For larger R, as the higher-order effects come in, the right-hand branch turns to the left via a fold. Such higher-order effects are not apparent from inspecting (3.10a, b), but they will be indicated and discussed in the numerical results in §3.2.3.

On account of the rapidly progressing algebraic complexity, a full evaluation of the higher growth rate coefficients becomes difficult. In the asymptotic limit $\eta^* \to \infty$,

however, certain simplifications are available. The following asymptotic expressions become useful in the evaluation of the expansion coefficients:

$$\left.\begin{aligned}
\alpha_c &= \lambda^{\frac{1}{3}}(1-\tfrac{7}{12}\pi^2\lambda^{-\frac{2}{3}}+\ldots),\\
R_c &= \lambda^{\frac{4}{3}}(3+\pi^2\lambda^{-\frac{2}{3}}+\ldots),\\
\omega_c &= -\frac{\sqrt{2}}{P}\lambda^{\frac{2}{3}}(1-\tfrac{5}{12}\pi^2\lambda^{-\frac{2}{3}}+\ldots),\\
\beta = R_c'' &= 24\lambda^{\frac{2}{3}}(1-\tfrac{13}{24}\pi^2\lambda^{-\frac{2}{3}}+\ldots),\\
\omega_c' &= \frac{\sqrt{2}}{P}\lambda^{\frac{1}{3}}(1-\tfrac{11}{6}\pi^2\lambda^{-\frac{2}{3}}+\ldots),\\
\omega_c'' &= -2\frac{\sqrt{2}}{P}\lambda^{\frac{2}{3}}(1-\tfrac{23}{3}\pi^2\lambda^{-\frac{2}{3}}+\ldots).
\end{aligned}\right\} \tag{3.12}$$

The actual algebraic simplifications come from assuming $\lambda^{\frac{1}{3}} \gg \pi$, which typically holds when η^* is larger than 10^4 where P is of order unity. In such a case we can neglect altogether terms that are associated with $\pi^2\lambda^{-\frac{2}{3}}$. In fact the condition $\lambda^{\frac{1}{3}} \gg \pi$ precludes the cases of low Prandtl number, where α_c is of order of π. Further simplifications lead to

$$\begin{aligned}
\sigma_3 = \frac{9\lambda^{\frac{4}{3}}}{4(1+P)^2\hat{A}^4}\Bigg[&\tfrac{\sqrt{2}}{3}(1-P^{-2})\left(\frac{\lambda^{-\frac{1}{3}}}{\pi^4}\right)\hat{A}^4\\
&+(\tfrac{\sqrt{2}}{24}P^{-2}(1+P)^3\frac{\lambda}{\pi^8}\hat{A}^4+128\sqrt{2}(1-P)\lambda^{-\frac{1}{3}}\hat{A}^2)\left(\frac{\alpha-\alpha_c}{\alpha_c}\right)\\
&+8\sqrt{2}P^{-1}(3-P)(1+P)\frac{\lambda}{\pi^4}\hat{A}^2\left(\frac{\alpha-\alpha_c}{\alpha_c}\right)^2-1472\sqrt{2}(1-P)\lambda\left(\frac{\alpha-\alpha_c}{\alpha_c}\right)^3\Bigg]
\end{aligned} \tag{3.13}$$

and

$$\begin{aligned}
\sigma_4 = \frac{27\lambda^2}{8(1+P)^3\hat{A}^6}\Bigg[&\tfrac{64}{3}(1+P)^2\lambda^{-\frac{4}{3}}\hat{A}^4+\frac{1}{36\pi^8}P^{-1}(1+P)^2(1-P^{-2})\hat{A}^6\\
&+\left(\frac{16}{3\pi^4}P^{-2}(1-2P)(1+P)(1-P)^2\hat{A}^4+\tfrac{1}{288}P^{-3}(1+P)^5\frac{\lambda^{\frac{4}{3}}}{\pi^{12}}\hat{A}^6\right)\left(\frac{\alpha-\alpha_c}{\alpha_c}\right)\\
&+\left(6144(1-P)^2\hat{A}^2+\tfrac{1}{6}P^{-2}(1+P)^2(-6P^4+4P^3-P^2+8P+3)\frac{\lambda^{\frac{4}{3}}}{\pi^8}\hat{A}^4\right)\left(\frac{\alpha-\alpha_c}{\alpha_c}\right)^2\\
&+P^{-1}(1+P)(3858-1213P+1518P^2)\frac{\lambda^{\frac{4}{3}}}{\pi^4}\hat{A}^2\left(\frac{\alpha-\alpha_c}{\alpha_c}\right)^3\\
&-2048(41-52P+41P^2)\lambda^{\frac{4}{3}}\left(\frac{\alpha-\alpha_c}{\alpha_c}\right)^4\Bigg].
\end{aligned} \tag{3.14}$$

Inspecting (3.13) and (3.14), we observe that the signs of σ_3 and σ_4 are strongly influenced by the first-order asymmetry terms proportional to $(\alpha-\alpha_c/\alpha_c)$. For both σ_3 and σ_4 the contribution to the asymmetry terms has strong dependence on the amplitude $\hat{A}$. By inspecting the expressions, it is apparent that when $\hat{A}$ is larger than a certain critical value (also see figure 4), both σ_3 and σ_4 become positive for $\alpha > \alpha_c$ and negative for $\alpha < \alpha_c$.

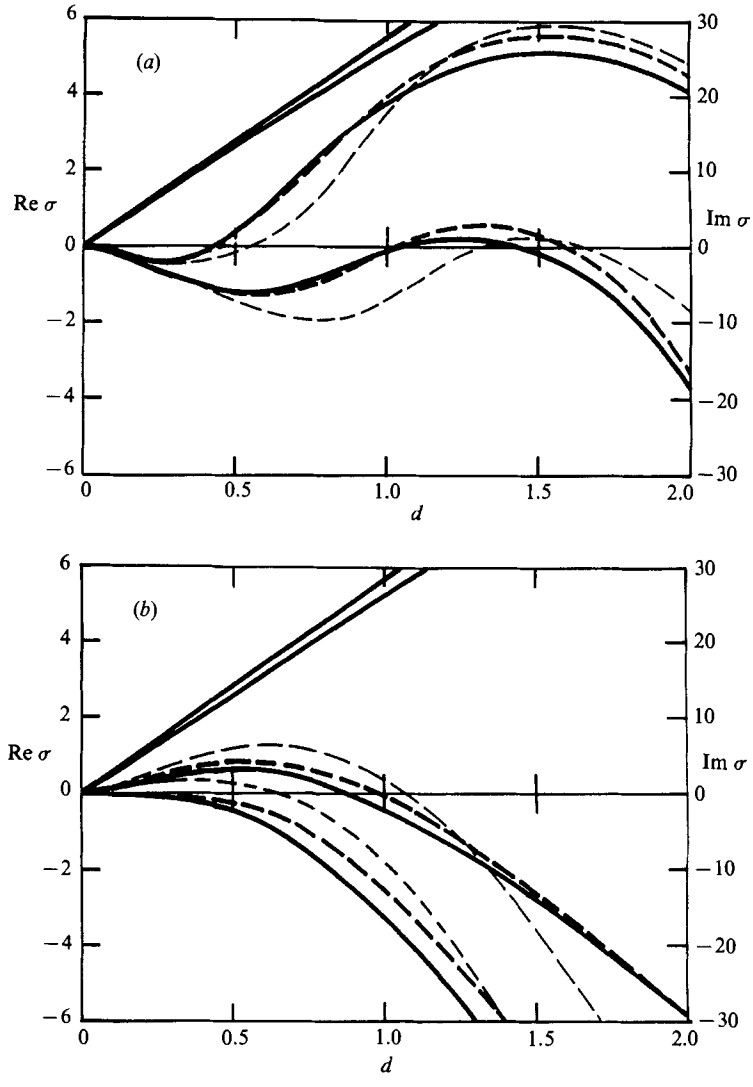

FIGURE 2. A comparison of the growth-rate dependence on the wavenumber modulation parameter for (*a*) the right-hand and (*b*) the left-hand branch of the stability limit.

3.2.3. *Numerical results*

Here we provide some interesting comparisons of the analytical results from the solvability condition with the fully nonlinear results from the earlier Galerkin formulation. Figure 2(*a*, *b*) shows a family of curves corresponding to the case $P = 1$, $\eta^* = 2.8 \times 10^3$ and $R = R_c + 2.82 \times 10^3$. The two figures contrast the typical asymmetry behaviour of the growth-rate variation with d on the two half-bands of α_c. In each figure, results from two different α values are shown: in figure 2(*a*) $\alpha = 10.6$ (lower family of curves) and 10.3 (upper family of curves); figure 2(*b*) shows $\alpha = 8.8$ (lower family) and 8.5 (upper family). The solid curves represent solutions from the Galerkin method; the heavy dashed curves represent solutions from (2.8); and the thin dashed curves represent solutions from (3.6). The solutions from (2.8) agree with those from the Galerkin method reasonably well. The qualitative

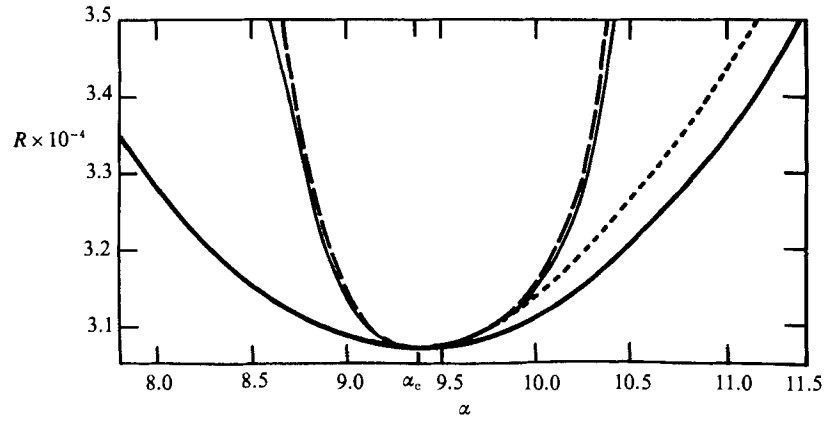

FIGURE 3. The stability limit in the α versus R plane for $P = 1$ and $\eta^* = 2800$.

behaviours of the results from all three different methods appear similar. Other than the accuracy concern, therefore, the simplified equation (3.6) has retained the essential instability properties. The straight curves shown in the figures are the σ_i value corresponding to the Galerkin formulation (see Or & Busse 1987). Note that in the Galerkin scheme the imaginary part of the eigenvalue was formulated in terms of the drift rate, rather than the frequency. The frequency modulations appear to be dominated by the zeroth-order effect, all three frequencies appear indistinguishable. In figure 2(*a*), the curve corresponding to $\alpha = 10.3$ appears to lie quite close to the stability limit. At this limit the curve will be tangent to the d-axis at a finite value of modulation denoted by d^*. Figure 3 shows the corresponding stability diagram in the (R, α)-plane for the same P and η^* as in figure 2. The stability limit corresponding to (2.8) is shown as the dashed curves. The left-hand branch of the stability limit is determined by the sign change of σ_2. The right-hand branch of the stability limit that is due to sign change in σ_2 is shown as the dotted curve. Note the strong asymmetry of these two branches with respect to α_c. On the right, preceding the dotted curve is a dashed curve typically corresponding to a finite value of d^*. The dashed curve marks the real stability limit. The more accurate stability limit determined from the Galerkin method appears as the thin solid curves in the figure. Again reasonably good agreement between the analytical and the Galerkin is shown from the stability diagram. On the right half-band of the stability diagram, it is natural to inquire how the dashed branch and the dotted branch of curves are connected. We magnify the region where these two curves meet. Figure 4(*a*) reveals that in fact the dashed limit emerges from the dotted limit at a finite amplitude. Thus for R less than the value marked by point L, no finite-d effects can be expected. Within the numerical resolution, however, it is difficult to determine whether the two curves intersect at a finite angle or are tangent to each other. At point L, d^* is non-zero. Near point L, the growth rate variation with d exhibits a double peak feature, as figure 4(*b*) shows. In the figure, the three curves denoted by A, B and C correspond respectively to $\alpha = 9.7186$, 9.7188 and 9.7190. For all three curves, $R = 30938$.

The features of the instability just described persist over a wide range of finite η^* that is of the order of 10^2 or larger, except when the Prandtl number becomes small (see below). To illustrate more about the growth-rate behaviour as well as its dependence on Prandtl number, we consider an example in which the growth-rate coefficients are evaluated through (3.7), (3.8) and (3.9). Near the critical condition,

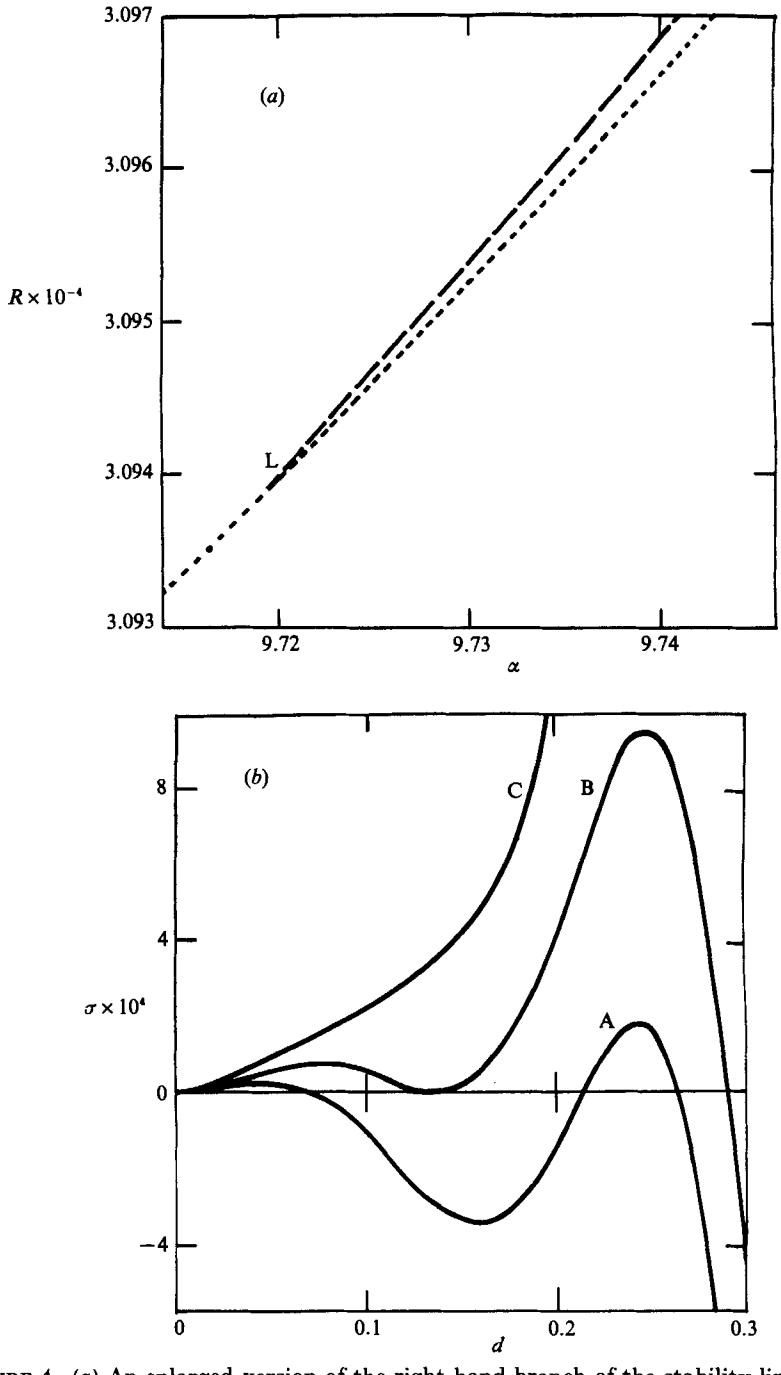

FIGURE 4. (*a*) An enlarged version of the right-hand branch of the stability limit of figure 3 near the region where branching occurs; (*b*) the corresponding growth-rate dependence on the modulation parameter at a point in the region.

	$\alpha = \alpha_L^*$	$\alpha = \alpha_c$	$\alpha = \alpha_R^*$	$\alpha = \alpha_R^{**}$
	$P = 0.2$, $(R-R_c)/R_c = 2.31 \times 10^{-2}$, $d^* = 0.4$			
$\alpha-\alpha_c$	−0.210	0	0.423	0.454
σ_2	0	−6.638	−3.683	0
σ_3	−11.28	−10.04	25.25	16.09
σ_4	−5.791	−13.27	78.4	63.4
σ_5	36.9	1.323	−273.0	−351.4
σ_6	−0.116	68.1	−594.6	−1444.3
	$P = 1.0$, $(R-R_c)/R_c = 9.19 \times 10^{-2}$, $d^* = 1.5$			
$\alpha-\alpha_c$	−0.322	0	0.920	1.352
σ_2	0	−5.024	−13.27	0
σ_3	−7.235	0	21.98	35.74
σ_4	−12.96	0.036	26.42	28.8
σ_5	21.72	0.007	−44.9	−99.02
σ_6	37.6	−0.039	−62.65	54.73
	$P = 10$, $(R-R_c)/R_c = 4.10 \times 10^{-2}$, $d^* = 1.4$			
$\alpha-\alpha_c$	−1.331	0	0.790	1.028
σ_2	0	−0.979	−1.769	0
σ_3	−0.023	1.439	1.851	6.168
σ_4	−0.622	2.136	1.115	−21.37
σ_5	0.814	−4.308	−2.589	−106.2
σ_6	2.245	−6.922	5.832	578.3

TABLE 1. The lower-order Taylor-expanded growth-rate coefficients

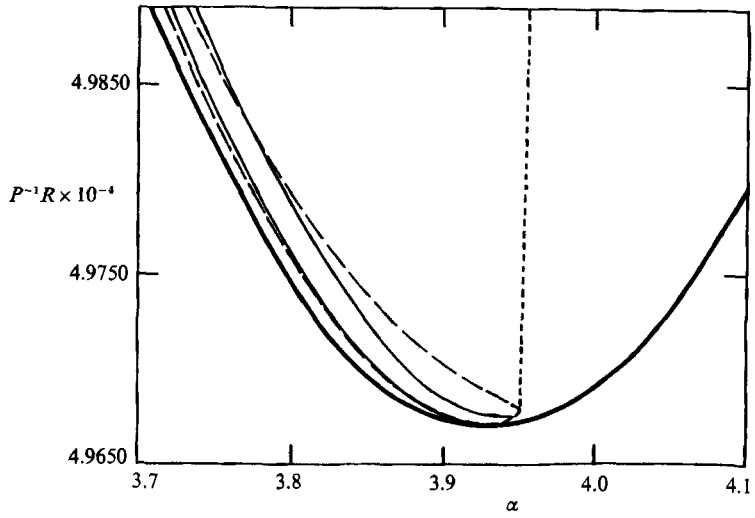

FIGURE 5. The stability limit in the α versus R plane for $P = 0.05$ and $\eta^* = 4000$.

table 1 shows the limiting values for the four wavenumbers on the band. From the table, α_L^*, α_R^* and α_R^{**} corresponds respectively to values on the left-hand dashed, right-hand dashed and right-hand dotted curves of figure 3. For larger P (not shown), the growth-rate behaviour remains similar. In all cases, the σ_3 and σ_4 values on opposite sides of α_c have opposite signs. On the right-hand dashed curve, σ_2 is negative while σ_4 is positive. The signs of σ_3 and σ_4 are roughly correlated.

A dramatic change in the characteristics of the instability limit occurs at low Prandtl number. Figure shows the stability region corresponding to a small Prandtl

number and a moderately high Coriolis parameter, such that $P = 0.05$ and $\eta^* = 4000$. The central band of stability practically disappears into the instability. The stable region is now a narrow strip leaning towards the far left of the primary neutral curve. The solid curves are obtained from the full Galerkin method. The dashed limits are obtained from evaluating (2.8). The two set of limits are qualitatively similar and reasonably close to each other. In both cases, the right limit corresponds to a finite d and the left limit corresponds to infinitesimal d. However, the values of d^* along the limit obtained from the Galerkin method are slightly smaller than those obtained from the solvability condition. Typically, the value of d^* obtained from the Galerkin method is about 0.1 and from the solvability condition it is about 0.2. The dotted curve which appeared as nearly straight line separates the unstable region into a stable region (left) and an unstable region (right) with respect to infinitesimal modulation. The above numerical results on the small-Prandtl-number limit can be better understood by relating to these results to the analytical results of the last section. For small P, as we recall, κ becomes very large. As α approaches a value close to 3.95, the term $1+\kappa[(\alpha-\alpha_c)/\alpha_c]$ tends to zero. Thus the dotted curve actually determines the limit where the denominator of (3.10*b*) changes sign. It renders the condition (3.10*b*) unable to be satisfied for all $R \geqslant R_c$, which implies that higher-order effects become important. Unlike the case shown in figure 3, in figure 5, above the fold, the finite-d instability is due to $\sigma_6 > 0$, where σ_4 is typically negative. Computing (3.7) shows that the growth rate coefficients for the region between the right-hand dashed limit and the dotted curve are such that σ_2 and σ_4 are both negative, but σ_6 is positive and is at least two order of magnitude larger than the corresponding σ_4. For example, at $\alpha = \alpha_c$ and $P^{-1}R = 49710$, $\sigma_2 = -4.95$, $\sigma_3 = 111.55$, $\sigma_4 = -722.1$, $\sigma_5 = 3.06 \times 10^3$, and $\sigma_6 = 3.77 \times 10^5$.

4. Concluding remarks and discussion

The paper provides an analytical extension of the results obtained from the earlier Galerkin method; the latter analysis appeared in Or & Busse (1987). Through the analytical approach, a broader view of the instability emerges. In particular, the parameter dependence of the stability limit can be sufficiently understood without having to compute numerous eigenvalue solutions. Two major effects have been identified in this paper: an onset of instability corresponding to finite Floquet parameter over the right-hand branch of the stability limit; and the shift of the stable band of solutions to the far left at low Prandtl number. For the latter effect, the familiar parabolic-shaped stable region actually turns into a narrow strip close to the left-hand branch of the primary neutral curve. Both effects appear to be a result of higher-order phenomena. These effects do not seem to occur in the several other better-known pattern-forming systems, in which the Eckhaus instability has been extensively studied.

The asymmetrical natue of these two effects seems to indicate that the frequency modulation of the disturbances plays an essential role in influencing the instability dynamics. Such frequency modulation depends intricately on the basic wavenumber, the modulation parameter and the amplitude of the wave, but no closed-form expression for the modulation is available. By examining the perturbational results, we are convinced that the frequency modulation exerts a dramatic influence on the higher-order growth rate. As $P \to 0$, the change in characteristics of the stability limit is not entirely surprising. Physically, in the low-Prandtl-number limit, the importance of the thermal nonlinearity shifts its importance to the hydrodynamic

nonlinearity. Thus the thermal Rossby waves in effect approach the inertial wave regime (see Busse 1983).

One last point we would like to mention is that even though the foregoing development appears quite cumbersome, the treatment does reflect the relative simplicity of a two-dimensional system as compared to a three-dimensional one. For example, a distorted stable region in the shape of a 'toe' has also appeared in an experimental study of wavy Taylor-vortex flow (see King & Swinney 1983). However, for such a system a solvability-condition approach is probably out of the question. To conclude, it is hoped that experimental techniques for measuring the wavelengths of the drifting thermal Rossby columns will soon become available so that the theory can be tested.

I am grateful to Professor F. H. Busse for many helpful discussions. The work was supported in part by the National Science Foundation, under the grant number AST-8796285; and in part by a grant from the Lawrence Livermore Laboratory.

REFERENCES

Azouni, M. A., Bolton, E. W. & Busse, F. H. 1986 Convection driven by centrifugal buoyancy in a rotating annulus. *Geophys. Astrophys. Fluid Dyn.* **34**, 301–317.

Benjamin, T. B. & Feir, J. E. 1967 The disintegration of wave trains on deep water. Part 1. Theory. *J. Fluid Mech* **27**, 417–430.

Busse, F. H. 1971 Stability regions of cellular fluid flow. *Instability of Continuous Systems, IUTAM Symp., Herrenalb 1969* (ed. H. Leipholz). Springer.

Busse, F. H. 1982 Thermal convection in rotating systems. In *Proc. 9th US National Congress of Appl. Mech., New York*, pp. 299–305. ASME.

Busse, F. H. 1983 A model of mean zonal flows in the major planets. *Geophys. Astrophys. Fluid Dyn.* **23**, 153–174.

Busse, F. H. & Bolton, E. W. 1984 Instabilities of convection rolls with stress-free boundaries near threshold. *J. Fluid Mech.* **146**, 115–125.

Busse, F. H. & Carrigan, C. R. 1974 Convection induced by centrifugal buoyancy. *J. Fluid Mech.* **62**, 579–592.

Busse, F. H. & Or, A. C. 1986 Convection in a rotating cylindrical annulus: thermal Rossby waves. *J. Fluid Mech.* **166**, 173–187.

Eckhaus, W. 1965 *Studies in Nonlinear Stability Theory*. Springer.

King, G. P. & Swinney, H. L. 1983 Limits of stability and irregular flow pattern in wavy vortex flow. *Phys. Rev.* A **27**, 1240–1243.

Kogelman, S. & DiPrima, R. C. 1970 Stability of spatially periodic supercritical flows in hydrodynamics. *Phys. Fluids* **13**, 1–11.

Kramer, L. & Zimmerman, W. 1985 On the Eckhaus instability for spatially periodic patterns. *Physica* **D16**, 221.

Nakaya, C. 1974 Domain of stable periodic vortex flows in a viscous fluid between concentric circular cylinders. *J. Phys. Soc. Japan* **36**, 1164–1173.

Newell, A. C. 1974 Envelope equations. Lectures in Applied Mathematics, vol. 15, pp. 157–163.

Newell, A. C. & Whitehead, J. A. 1969 Finite bandwidth, finite amplitude convection. *J. Fluid Mech.* **38**, 279–303.

Or, A. C. & Busse, F. H. 1987 Convection in a rotating cylindrical annulus. Part 2. Transition to asymmetric and vascillating flow. *J. Fluid Mech.* **174**, 313–326.

Riecke, H. & Paap, H. G. 1986 Stability and wake-vector restriction of axisymmetric Taylor vortex flow. *Phys. Rev.* A **33**, 547.

Stuart, J. T. & DiPrima, R. C. 1978 The Eckhaus and Benjamin–Feir resonance mechanisms. *Proc. R. Soc. Lond.* A **362**, 27–41.